Eur. Phys. J. D **62**, 309–325 (2011)
DOI: 10.1140/epjd/e2011-10584-7

THE EUROPEAN PHYSICAL JOURNAL D

Regular Article

Atom interferometry measurement of the atom-surface van der Waals interaction

S. Lepoutre[1], V.P.A. Lonij[2], H. Jelassi[1,3], G. Trénec[1], M. Büchner[1], A.D. Cronin[2], and J. Vigué[1,a]

[1] Laboratoire Collisions Agrégats Réactivité IRSAMC, Université de Toulouse-UPS and CNRS UMR 5589, 118 route de Narbonne, 31062 Toulouse Cedex 9, France
[2] Department of Physics, University of Arizona, Tucson, Arizona 85721, USA
[3] Centre National des Sciences et Technologies Nucléaires, CNSTN, Pôle Technologique, 2020 Sidi Thabet, Tunisia

Received 13 October 2010 / Received in final form 11 February 2011
Published online 25 March 2011 –

Abstract. Using a nano-scale grid as a phase-shifting component, an atom interferometer has been utilized to study atom-surface van der Waals (VdW) interactions. We report phase shifts on the order of 0.2 rad, with a few percent uncertainty. We also report the velocity-dependent attenuation of atomic de Broglie wave amplitude that occurs in conjunction with the observed phase shifts. From these data we deduce the strength of the VdW potential and its dependence on the atom-surface separation. We discuss how our measurements can be used to set limits on the strength of non-Newtonian gravity at short length scales and we discuss the possibility of measuring the atom-surface interactions over a larger range of atom-surface distances. We also compare our results to several theoretical predictions for the VdW potential of Li near a variety of surfaces.

1 Introduction

Diffraction of atoms by nano gratings has attracted attention recently because the diffraction amplitudes are sensitive to atom-surface van der Waals (VdW) interactions. In references [1–8] the relative intensities of several diffraction orders were studied, whereas in references [9,10] atom interferometers were used to measure the additional phase induced by a nano-grating. In this paper we show how both the modulus and the phase of the zeroth order diffraction amplitude can be reported from a single experiment. We used these data to measure the strength of the VdW potential at different atom-surface separations and to set experimental limits on possible Yukawa-type modification of Newtonian gravity at short length scales.

With a separated beam atom interferometer [11], almost any type of perturbation can be measured by transmitting one arm of the interferometer through an interaction region while the reference arm propagates freely. The modulus and the phase of the transmission amplitude can be determined from the interference signals. A variety of such experiments have already been done: atomic electric polarizabilities have been measured with interaction regions containing an electric field [12–14], complex scattering amplitudes have been measured with an interaction region containing a dilute gas [15–17], and in this paper we describe an experiment where one arm of the interferometer passes through a nanostructure. The resulting interaction depends on the atom-surface van der Waals potential [9,10].

Several previous experimental techniques have been used to measure atom-surface interactions. The study of the short-range ($r < 1$ nm, where r is the atom-surface distance) part of atom-surface interaction is well developed, the detection of atom-surface bound states by inelastic scattering experiments can give very accurate measurements and we refer the reader to the review paper by Hoinkes [18] for more details. However, inelastic scattering experiments do not give a direct access to the long range part of this interaction ($r > 1$ nm). In this range, atom-surface interaction is attractive and dominated by the dipole-dipole term, which behaves as $-C_3/r^3$. Such a potential may support a series of long-range bound states which are difficult to detect because of insufficient resolution and sensitivity. Laser spectroscopy of atoms interacting with a dielectric surface has already given access to the long-range part of the atom-surface interaction [19] but this spectroscopy is sensitive only to the difference of the interaction potentials corresponding to the different internal states of the atom that are coupled by the laser.

Atom optics experiments, such as atom diffraction from a nano grating, can be used to measure the long-range interaction of the atom in its ground state with the surface. The first experiment of this type was done in 1999 by Grisenti et al. [1], who measured the intensities of the various diffraction orders of a nano grating as a function of the atom velocity. Several similar experiments have been performed since then [4–6,8]. These experiments give access to the modulus of the diffraction amplitude but not to its phase which can be measured only by atom interferometry; this was done for the first time by Perreault and

[a] e-mail: jacques.vigue@irsamc.ups-tlse.fr

Cronin [9] in 2005 (see also [20,21]). We present here new results from an improved experiment of this type originally reported in [10].

There is a growing interest for the very long range part of the atom-atom, atom-surface and surface-surface interactions because of the Casimir effect and its connection to vacuum zero-point energy [22]. This effect has been detected by various experimental techniques: observation of the quantum reflection of atoms from a surface [23,24]; study of the vibration of a trapped Bose-Einstein condensate near a surface [25–27]. Towards the end of this paper (Sect. 3.6) we discuss how to study this long-range region by atom interferometry by adapting our experiment. First, we introduce the structure of this paper.

We describe the principle of our experiment in Sections 2.1 and 2.2. In Section 2.3, we describe our atom interferometer and we present experimental signals. We show experimental results for the modulus and the phase of the diffraction amplitude in Section 2.4. The phase of this diffraction amplitude presents an unexpected behavior: it does not vary as $1/v$, which is the classic behavior for a perturbation-induced phase shift.

In Section 3, we explain this behavior quantitatively by a numerical calculation and also by an analytic model. We show how the observed velocity dependence serves as a sensitive test of the dependence of the atom-surface interaction with the atom-surface distance r. If we assume a general form for the atom-surface potential of $-C_p/r^p$, we determine that $p = 2.9 \pm 0.2$, thus confirming that the dipole-dipole interaction, with $p = 3$, dominates the van der Waals (VdW) interaction in the range of distances to which our experiment is sensitive (Sect. 3.3). A large source of uncertainty in measurements of atom-surface interactions using nano gratings has traditionally been the lack of knowledge of the grating geometry (width and shape of the nano-bars). Thanks to a thorough analysis of the diffraction pattern, two of us (VPAL and ADC) [6] have been able to measure very accurately the geometrical parameters of the nano grating we have used. With this knowledge, we can use the measured phase to obtain the C_3 parameter for lithium atom interacting with a silicon nitride surface with 6% precision. In Section 3.4 we compare the measured C_3 parameter to theoretical predictions based on a formula due to Lifshitz [28,29]. Using the analytical model explained in Section 3.5, we can gain some physical insight into the behavior of our experiment. Based on this analytic model we discuss how to measure atom-surface interactions in the Casimir-Polder regime using larger nano-structures in Section 3.6. Finally, in Section 3.7 we show how our experiment can be used to test possible modifications of gravity at very short range. Assuming a Yukawa potential term, if the range parameter is close to 2 nm, our experiment appears to be a competitive test with other experiments measuring Van der Waals interaction and we briefly discuss possible improvements. However, a considerably better sensitivity has been achieved with neutron interferometry and we explain why.

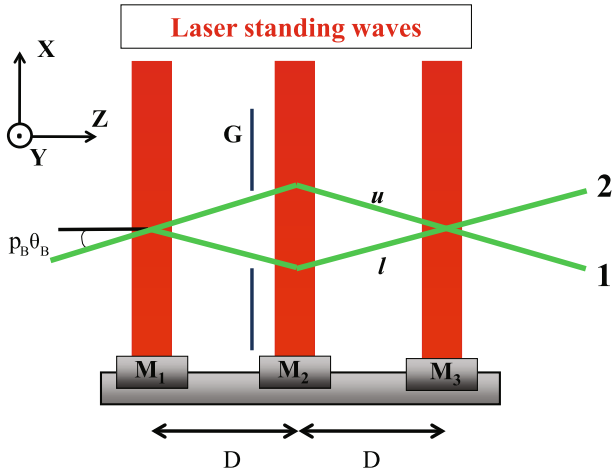

Fig. 1. (Color online) Schematic top view of our atom interferometer: after a strong collimation by narrow slits (not shown here), a supersonic beam of lithium is diffracted three times by laser standing waves in the Bragg regime. The laser standing waves are obtained by reflecting a laser beam on the mirrors M_i ($i = 1-3$) and the Bragg regime requires an angle of incidence of the atomic beam equal to $p_B\theta_B$. The distance D between consecutive laser standing waves is $D = 0.6$ m. Each atom can go from the source to the detector by two paths labeled u and l which interfere on the detector. A detection slit (not shown) selects one of the output beams labeled 1 and 2, which carry complementary fringe signals. A nano grating G can be inserted just before the second standing wave, at the position where the distance between the two interferometer arms u and l is largest, of the order of 100 μm. This figure defines the axis $\mathbf{X}, \mathbf{Y}, \mathbf{Z}$ used in the analysis.

2 Principle and results of the experiment

We have described our atom interferometer in reference [30] and we recall here only the main features. A supersonic beam of lithium seeded in a carrier gas is highly collimated. The collimated beam then crosses three quasi-resonant laser standing waves which diffract the lithium atoms, thus forming a Mach-Zehnder atom interferometer (see Fig. 1). Atomic diffraction occurs in the Bragg regime which has the advantage of producing only two beams, of orders 0 and p_B with a tunable amplitude ratio: the order p_B is chosen by incidence angle of the atom beam on the laser standing waves, equal to $p_B\theta_B$, with $\theta_B = \lambda_{dB}/\lambda_L$, λ_{dB} being the atom de Broglie wavelength $\lambda_{dB} = h/(mv)$ and λ_L the laser wavelength. In this experiment we have used both first order ($p_B = 1$) and second order ($p_B = 2$) Bragg diffraction. The amplitude ratio between the orders 0 and p_B is tuned by the parameters of the standing wave (laser beam diameter and power density, laser frequency detuning). A detection slit selects the output beam which is detected by a hot-wire detector. A very important point is that the two interferometer arms are well separated in space, near the second laser standing wave, and we are thus able to perturb the propagation of only one arm and to detect the perturbation on the interference signals.

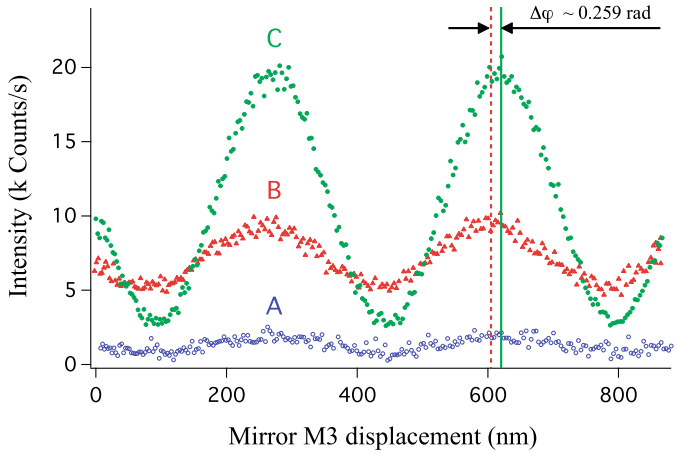

Fig. 2. (Color online) Atom interference fringes recorded with (A) both arms (visibility $\mathcal{V}_A = 32\%$), (B) one arm ($\mathcal{V}_B = 34\%$), or (C) neither arm ($\mathcal{V}_C = 72\%$) passing through the nano grating. The mean velocity of the lithium beam is equal to $v = 744 \pm 18$ m/s. The counting period is 0.1 s per data point.

2.1 Simple model of the atom interferometer signal

A complete model of our Mach-Zehnder interferometer is very complex because the diffraction by the collimation slits is intermediate between the near-field and the far-field regimes [31,32]. A plane-wave model of the interferometer is however sufficient to calculate the effect of a nano grating on the interferometer signals. With this simplification, the output signal intensity results from the interference of two arms of the interferometer (see Fig. 1) described by amplitudes a_u and a_l corresponding to the upper and lower arm respectively:

$$I = |a_u + a_l \exp(i\varphi)|^2 \quad (1)$$

where the phase is the sum of three terms $\varphi = \varphi_0 + \Delta\varphi + \varphi_{noise}$. The induced phase $\Delta\varphi$ is the result of a phase shift applied to one of the interferometer arms by an interaction, in this case a nano grating. We introduce the phase φ_{noise} to describe all the fluctuating phases which are responsible for reducing fringe visibility (see Sect. 2.6).

The phase is given by $\varphi_0 = 2p_B k_L (2X_2 - X_1 - X_3)$, where $k_L = 2\pi/\lambda_L$ is the wavevector of the laser used for atom diffraction. φ_0 depends on the positions X_i of the mirrors M_i ($i = 1, 2, 3$) of the three laser standing waves ($\mathbf{X}$ is normal to the mirror surface, see Fig. 1). By displacing mirror M_3, we observe oscillations in the output signal as a function of the mirror position X_3. The position of the mirror is controlled by a piezo drive. In order to have precise knowledge of the displacement of mirror M_3, we have built a Michelson interferometer involving M_3 and a fixed mirror. This interferometer, which is completely under vacuum, is operated with an helium-neon laser. The recorded Michelson fringes provide a measurement of X_3 with a twenty times better sensitivity than previous methods using an optical Mach-Zehnder interferometer. In this way, we have an accurate calibration of the displacement of mirror M_3 and this information is needed to plot the atom interference fringes shown in Figure 2.

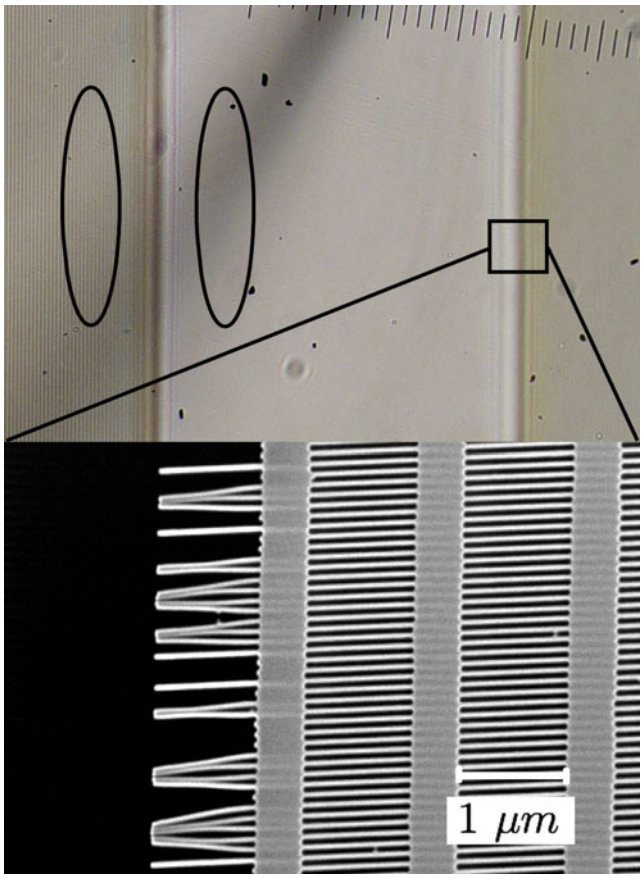

Fig. 3. (Color online) (top) Optical microscope image of the interaction grating. The nano-structure appears as a gray membrane. A 200 μm wide gap has been made in the membrane to allow one or both interferometer arms to pass though the grating without interacting with the nano-structure. The two ovals represent schematically the two arms of the interferometer, roughly to scale in the horizontal direction but not in the vertical direction (in this direction the arm extension is close to 1 mm. (bottom) Electron microscope image of the nano-structure. The 100 nm period nano-structure is visible as well as the 1.5 μm period support structure. A small part of the gap is visible to the left.

2.2 The transmission nano grating used as phase shifting component

Transmission nano gratings with periods on the order of 100 nm have been used in atom interferometry experiments [33,34] both as coherent beam-splitters and as phase shifting elements. The phase shift arises due to the van der Waals atom-surface interaction between the atoms and the grating walls.

In the present work, we use the same nano grating used by Perreault et al. [7,9,21] which consists of a series of regularly spaced openings in a SiN_x membrane. To describe the nano-grating, we use a $\mathbf{x}$ axis perpendicular to the nano-bars and a $\mathbf{y}$ parallel to these bars. The width w of the openings is about $w = 53 \pm 1.2$ nm and the nano grating period d_x is $d_x = 100 \pm 0.1$ nm, see Figure 3. A periodic support structure in the perpendicular

direction keeps the bars from sticking together. The period of this structure is $d_y = 1.5$ μm and its open fraction β_y is close to $\beta_y = 0.67 \pm 0.04$. The membrane thickness L is $L = 110 \pm 5$ nm.

In the current experiment, the grating is oriented with the nano-bars horizontally (as in Fig. 3), i.e. the grating **x** axis is roughly parallel to the interferometer **Y** axis, such that diffraction from this nano-structure deflects atoms out of the plane of the interferometer. A 200 μm wide gap in the nano-structure allows one or both interferometer arms to pass through without interacting with the nanostructure. We give a detailed description of the effect of the nano gratings on an atomic beam in Section 3.

When one of the interferometer arms interacts with a nano grating, there is diffraction due to the 100 nm period nano-structure as well as the 1.5 μm period support structure. The result is a series of diffracted beams with momenta in the x and y directions with their complex diffraction amplitudes noted $A(p_{Gx}, p_{Gy})$.

We consider first the case with a nano grating introduced on only one of the interferometer arms, for example the arm labeled u as shown in Figure 1. When the nano grating is introduced in this beam, the $(0,0)$ order diffracted beam replaces the incident beam and the amplitude a_u of this beam is replaced by $a_u A(0,0)$. All the diffracted beams with $(p_{Gx}, p_{Gy}) \neq (0,0)$ propagate inside the interferometer and their contribution to the signal is proportional to their degree of transmission by the detection slit, denoted $T_u(p_{Gx}, p_{Gy})$. Because the diffracted beams make a non-vanishing angle with the main output beams of the interferometer, the interference of these stray beams with the main output beams is completely washed out by the integration over the detector surface and also by the integration over the atom velocity distribution.

The signal can now be written:

$$\begin{aligned} I &= |a_u A(0,0) + a_l \exp(i\varphi)|^2 + I_{sb,u} \\ \text{with } I_{sb,u} &= \sum_{p_{Gx}, p_{Gy} \neq (0,0)} a_u^2 \left|A(p_{Gx}, p_{Gy})\right|^2 \\ &\quad \times T_u(p_{Gx}, p_{Gy}). \end{aligned} \tag{2}$$

Here $I_{sb,u}$ designates the total intensity of the detected stray beams in this configuration. This signal can also be written in the usual form, $I = I_m[1 + \mathcal{V}_m \cos\varphi_m]$ with modified parameters:

$$\begin{aligned} I_m &= a_u^2 |A(0,0)|^2 + a_l^2 + I_{sb,u} \\ \mathcal{V}_m &= \frac{2 a_u a_l |A(0,0)| \langle \cos\varphi_{noise} \rangle}{a_u^2 |A(0,0)|^2 + a_l^2 + I_{sb,u}} \\ \varphi_m &= \varphi_0 - \Phi_0 \end{aligned} \tag{3}$$

where we have noted $\Phi_0 = \arg(A(0,0))$. If one assumes that the arm amplitudes are initially balanced ($|a_u| \approx |a_l|$), the introduction of the nano grating always reduces the fringe visibility i.e. $\mathcal{V}_m < \mathcal{V}_0$, even if the detected stray beam intensity $I_{sb,u}$ is small. This is because the nano gratings are absorptive and attenuate the transmitted beam. Since the interferometer is usually not perfectly balanced ($|a_u| \neq |a_l|$), the modified visibility $\mathcal{V}_m$ will depend on which arm passes through the nano grating.

It is possible to extract directly the modulus $|A(0,0)|$ of the diffraction amplitude from the knowledge of the modified intensity and visibility:

$$|A(0,0)| = \frac{I_m \mathcal{V}_m}{I_0 \mathcal{V}_0} \tag{4}$$

where I_0 is the mean intensity when both arms go through the nanograting gap. This expression gives the modulus of the part of the atom beam that contributes to the detected fringes. Furthermore, the background count rate from our detector does not affect equation (4).

The case with the nano grating located on the lower atomic beam is completely analogous. The main differences concern the visibility because the detected stray beam intensities $I_{sb,u}$ and $I_{sb,l}$ may be substantially different. In addition the equation for the phase now becomes:

$$\varphi_m = \varphi_0 + \Phi_0. \tag{5}$$

When the nano grating is introduced on both interferometer arms, the situation is more complex, with more stray beams. We will not give any equations for this case but we point out a few interesting properties:

- both amplitudes a_u and a_l are multiplied by $A(0,0)$, so that the fringe phase must be the same as when there was no nano grating on the interferometer arms;
- the two beam amplitudes are now balanced, exactly as when there was no nano grating on the interferometer arms. If there were no stray beams, the visibility should be back to its initial value $\mathcal{V}_0$. The no-stray beam hypothesis is obviously not realistic but, nevertheless, in some experiments, we have observed a small increase of the visibility with respect to the case where only one arm was passing through the nano grating;
- we have already said that the nano grating **x** axis is not exactly coincident with the **Y** axis of the interferometer. In case of an exact coincidence, some stray beams would fulfill the Bragg condition and would be diffracted by the laser standing waves, thus forming supplementary interferometers. A very small angle between the nano grating axis and the interferometer axis is sufficient to prevent this possibility and, as we have not aligned precisely the nano grating axis with respect to the interferometer axis, we think that the signals due to this supplementary interferometers can be neglected.

2.3 Interpreting the interferometer signals

The nano grating is on a translation stage along the **X** direction and it is thus possible to have either 0, 1 or 2 arms going through the nano grating and, as the arms can go through the nano grating on both sides of the window, we can explore the following five different situations, using the notations of Figure 1.

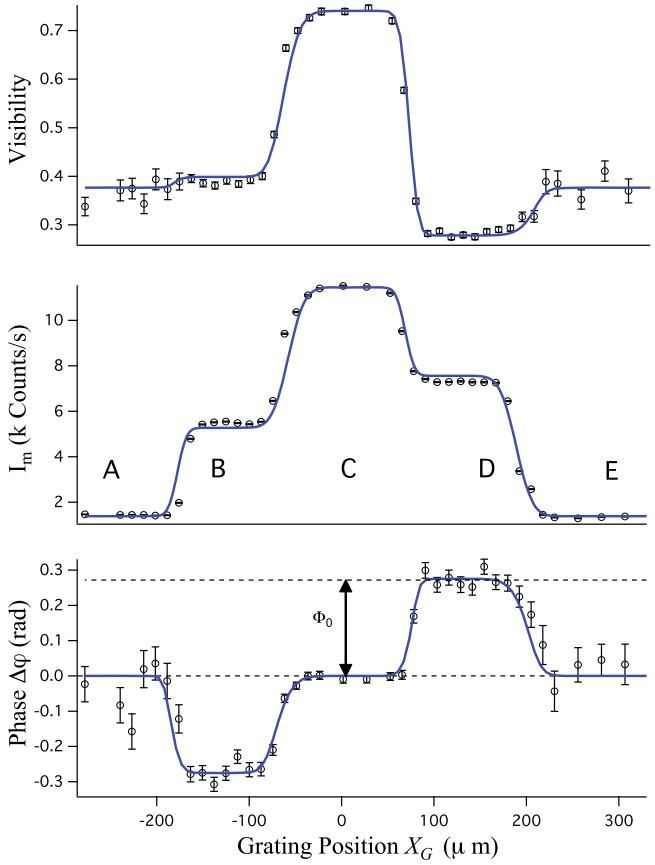

Fig. 4. (Color online) The visibility $\mathcal{V}$ of the interference fringes, the mean signal intensity I_m and the phase shift $\Delta\varphi$ are plotted as a function of the interaction-nano grating position X_G, for a lithium beam velocity $v = 744 \pm 18$ m/s. The reference position corresponds to $X_G = 0$. This position belongs to the configuration C with both interferometer arms going unaffected through the nano grating gap. When $90 \lesssim |X_G| \lesssim 175$ μm, one arm goes through the nano grating while the other arm propagates through the nano grating gap (configurations B or D) and we observe opposite phase shifts. The mean intensity and the fringe visibility are reduced, as discussed in the text. When $|X_G| \gtrsim 200$ μm (configurations A or E), both arms go through the nano grating and the phase shift is close to 0, as expected. The asymmetry between the intensities and visibilities in configurations B and D come from imbalance in the amplitudes of the two paths (u) and (l) (see Fig. 1). Configuration D corresponds to intercepting atomic beam (l) which is broadened by velocity-dependent diffraction. Therefore region D is slightly wider than region B. The best fit (which neglects the latter effect) is represented by the continuous line.

(A) Both arms go through the nano grating on one side of the gap;
(B) arm u goes through the nano grating and the other arm goes through the gap;
(C) both arms go through the gap;
(D) arm l goes through the nano grating and the other arm passes through the gap;
(E) both arms go through the nano grating on the other side of the gap.

The results are shown in Figure 4.

The cases (B) and (D) provide two measurements of the interaction of the nano grating with the atomic beam from which we can deduce the zero-order amplitude and phase. These two measurements test different parts of the nano grating but they are in very good agreement: this is proof of the very good homogeneity of the nano grating geometrical parameters. Finally, cases (A) and (E) enable us to verify the prediction of a vanishing phase shift when the two atomic beams go through the nano grating but, as the mean intensity I_m and the visibility $\mathcal{V}_m$ are both considerably reduced with respect to case (C), the phase sensitivity is reduced and this test is not very accurate.

The procedure we used to characterize the effect of the nano grating is as follows. In a first step, we align our atom interferometer with the two arms going through the nano grating gap (configuration C). In this configuration we routinely achieve a fringe visibility $\mathcal{V}_0$ close to 70% and a detected mean intensity I_0 of the order of $(2-10) \times 10^4$ counts/s. The value of I_0 is stable during an experimental run but this value is determined by the choice of the supersonic beam source parameters (choice of carrier gas and pressure, oven temperature) and by the slit widths (collimation and detection slits). A typical fringe signal is plotted in Figure 2.

Then, we studied the five configurations (A) though (E) and recorded interference fringes in all cases. From the recorded fringes, we have measured the mean intensity I_m, the fringe visibility $\mathcal{V}_m$ and the phase-shift $\Delta\varphi$. In Figure 4, we have plotted these three quantities as a function of the nano grating position X_G.

Because of attenuation by the nano grating, the mean intensity is reduced when one arm of the interferometer goes through the nano-structure (cases B and D). When both arms pass through the nanostructure, the mean intensity is even further reduced. The visibility is also affected by the nano grating; attenuation and stray beams greatly decrease the visibility in cases B and D (as compared to C). It varies only slightly when going from B to A or from D to E and in some cases the visibility is larger when the two arms go through the nano grating than when only one goes through it. We clearly observe all the effects predicted by our analysis in Section 2.2. The change $\Delta\varphi$ in the measured phase is clearly visible when going from C to B or to D and this change is a measurement of the argument Φ_0 of $A(0,0)$. An accurate measurement of this phase-shift requires careful control for the phase drift of the fringe signal. We explain this in Section 2.5.

Table 1. For each carrier gas, we give the measured mean velocity v of the lithium beam.

Carrier gas	Velocity v (m/s)
Kr	744 ± 18
Ar	1062 ± 20
Ar 50%–He 50%	1181 ± 27
Ne	1520 ± 38
Ar 10%–He 90%	2400 ± 100
He	3300 ± 82

2.4 Velocity dependence of the zeroth order diffraction amplitude

The lithium beam mean velocity can be varied by changing the carrier gas [17] and we have thus covered the 750−3300 m/s range (see Tab. 1). The atomic beam mean velocity v was measured by Bragg diffraction rocking curve and by Doppler sensitive laser induced fluorescence.

In the first method, we record the intensity of the atomic beam transmitted through a laser standing wave as a function of the rotation of the mirror producing this standing wave. We observe two intensity dips when the Bragg condition for order $p_B = \pm 1$ is fulfilled. The difference in mirror rotation angles between the two peaks gives us the Bragg angle, from which we deduce the beam mean velocity. The signals are similar to those presented in Figure 3 of reference [30].

In the second method, the atom is excited by a laser crossing the atomic beam with an angle near 45° and the fluorescence intensity is recorded as a function of the laser frequency. We thus get the fluorescence intensity as a function of the Doppler shift. The two methods are in good agreement and give the mean velocity with a few percents uncertainty (see Tab. 1).

The maximum distance between the interferometer arms occurs near the second laser standing wave and, when using first order Bragg diffraction, the distance between the centers of the two arms is about 100 μm for an atom velocity $v = 1000$ m/s. This distance is sufficient to let us position a nano-grating such that it intercepts only one arm without disturbing the other one. However, when the velocity v increases, this distance decreases like $1/v$. When the velocity is larger than 2000 m/s, the distance becomes too small to perform a clean experiment. In this case (i.e. the two largest velocities of Tab. 1), we used second order Bragg diffraction, thus doubling this distance. However, when using second order Bragg diffraction, we have not been able to fully suppress the stray atomic beams due to residual first-order diffraction on the laser standing waves and the experiment was less ideal than when using first-order diffraction.

Figure 5 shows the measured phase Φ_0 of the zeroth order diffraction amplitude as a function of the mean velocity of the atom beam (the values are collected in Tab. 2). The velocity dependence is due entirely to the VdW interaction as, in the absence of atom-surface interactions, the phase Φ_0 should vanish. The data is shown on a log-log plot and it appears to lie on a line in this plot. This suggests a power-law behavior, in fact $\Phi_0 \propto v^{-0.49}$. This particular velocity dependence is unusual in atom optics; we will give an explanation for this dependence in Section 3.

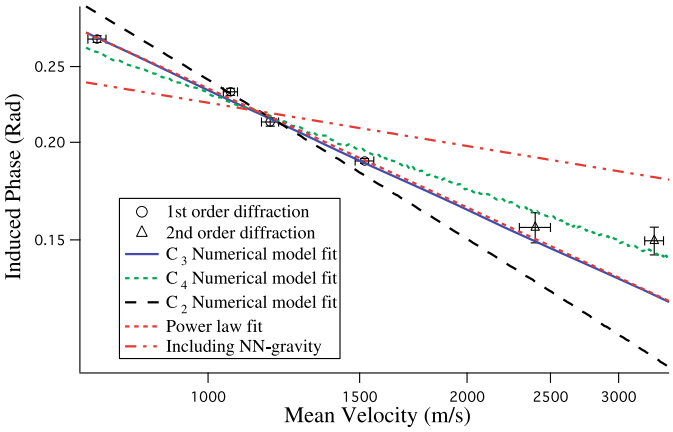

Fig. 5. (Color online) Phase Φ_0 of the zeroth order diffraction amplitude as a function of the atomic beam mean velocity v. The data closely follow a power law ($\Phi_0 \propto v^{-0.49}$) indicated by the dashed red line. The data were also fit using the model described in Section 3. The black, blue and green lines correspond to fits using a potential shape $V = -C_p/r^p$ with $p = \{2, 3, 4\}$ respectively. The rightmost two data points were obtained using second order Bragg diffraction by the laser standing waves. In this condition there is still a small amount of first order Bragg diffraction which causes a significant systematic error.

Table 2. Experimental results: for each experiment, we recall the atomic beam mean velocity v and we give the measured values of the phase Φ_0 in mrad and of the modulus $|A(0,0)|$ of the zeroth order diffraction amplitude. The 1σ statistical error bars of are estimated from the dispersion of large series of measurements. These results are discussed in the next part.

Velocity v (m/s)	Φ_0 (mrad)	$\lvert A(0,0)\rvert$
744 ± 18	271.1 ± 3.3	0.2459 ± 0.0015
1062 ± 20	232.1 ± 3.5	0.2594 ± 0.0020
1181 ± 27	212.4 ± 2.2	0.2602 ± 0.0025
1520 ± 38	189.3 ± 2.0	0.2699 ± 0.0041
2400 ± 100	155.6 ± 5.9	0.2716 ± 0.0019
3300 ± 82	149.6 ± 4.8	0.2805 ± 0.0025

Using equation (4), we have also determined the modulus $|A(0,0)|$ of the zeroth order diffraction amplitude. That is, we can determine the modulus of the part of the beam that actually contributes to the fringes. The results, also collected in Table 2, are plotted in Figure 6. We want to point out that this interferometric technique gives a very small uncertainty, near 0.5% in the best cases but it can be applied only to the zeroth order of diffraction amplitude. The dependence on velocity is once again entirely due to the van der Waals interaction.

We can explain the modulus of the diffraction amplitude by considering both diffraction from the nano-bars,

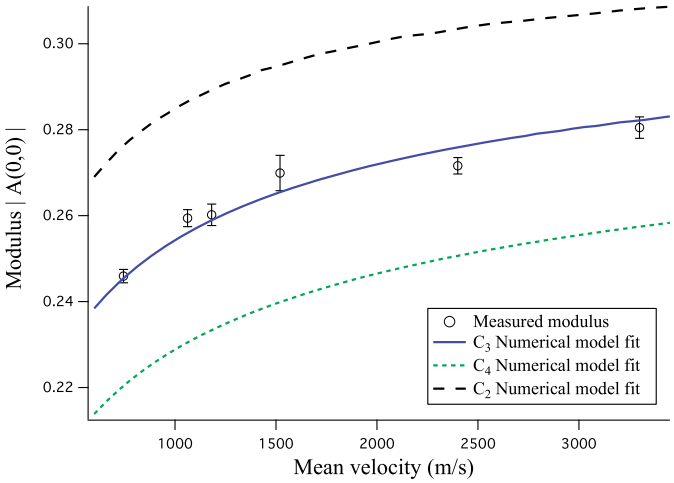

Fig. 6. (Color online) Modulus $|A(0,0)|$ of the zeroth order diffraction amplitude as a function of the atomic beam mean velocity v. The data are based in equation (4). The method by which $|A(0,0)|$ is calculated is explained in Section 3.3. The black, blue and green lines correspond to calculations using a potential shape $V = -C_p/r^p$ with $p = \{2,3,4\}$ respectively. The $p = 3$ fit has only one free parameter: β_y^{fit}, the support structure open-fraction. For the $p = 2$ and $p = 4$ calculations, β_y is fixed to the value found from the $p = 3$ fit in order to highlight the effect of the shape of the potential on the modulus.

as described in Section 3.3, as well as diffraction from the support structure (see Fig. 3). We use the same numerical model to fit the modulus as we used to fit the phase data. The geometric parameters for the grating are taken from reference [6] and the value for C_3 is obtained from the phase data. The fit shown in Figure 6 has only one free parameter: the open-fraction of the support structure (see Sect. 3.2). The open-fraction of the support structure found from the fit in Figure 6 is $\beta_y^{fit} = 0.61 \pm 0.01$. However if we determine the support structure open-fraction from SEM images like Figure 3, we find $\beta_y^{SEM} = 0.67 \pm 0.04$. The discrepancy could be due to an additional source of contrast-loss when the grating is introduced to one arm of the interferometer, i.e. the parameter φ_{noise} in equation (3) need not be the same in both the numerator and the denominator of equation (4). This additional random variation in the phase can be caused by a distribution of grating geometric parameters across the different regions of the grating that we are sampling.

In addition to the fit based on the potential $V = -C_p/r^p$ with $p = 3$, we also show fits using $p = 2$ and $p = 4$. These fits have no free parameters, as we determined C_p from the phase data and use the support structure open-fraction, β_y^{fit}, found from the $p = 3$ fit. These plots highlight the fact that the modulus, just like the phase is highly sensitive to the shape of the potential. If the additional loss in visibility that cause the discrepancy between β_y^{fit} and β_y^{SEM} were better understood, measurements of the modulus could better constrain the shape of the potential.

2.5 Phase drift

As in our previous experiments [17,35], the phase of the interferometer signal drifts with time. In order to improve the measurement accuracy, we alternate between recording fringes with and without the perturbation. We first record fringes at a reference position (taken as the origin $X_G = 0$) corresponding to the middle of configuration C, with two arms going through the nano grating gap. Then we measure fringes at a different position X_G and finally again at $X_G = 0$. The phase shift due to the nano grating is taken equal to the difference between the phase measured with the nano grating at X_G and the mean of the two phases measured at $X_G = 0$ just before and after. The phase measured with the nano grating at the $X_G = 0$ reference position drifts with time and a typical variation is about 1−2 rad during a two-hour long series of measurements.

This phase drift corresponds a very small displacement of the mirrors of the three laser standing waves, as a 53 nm variation of $(2X_2 - X_1 - X_3)$ is sufficient to induce a 1 rad phase shift. This drift appears to have at least two origins. There is a continuous trend which, during a series of measurements, slows down with time. The slowing down behavior suggests a creep phenomenon (see for example [36]) which are well known to appear with piezo-actuators. This creep effect is not due to the piezo-actuator of mirror M_3 as we measure the position of this mirror with the Michelson interferometer described above. There is also an oscillation of the phase with a period ca. 20 min and an amplitude ca. 100 milliradians. This oscillation is clearly correlated to an oscillation of the temperature of the refrigerated water which flows through baffles of the oil diffusion pumps pumping the interferometer vacuum chamber: this temperature oscillates with a 3 K amplitude and with the same period. We think that the metal bar supporting the three laser standing wave mirrors, which is coupled to these baffles by radiation, may be slightly distorted by the induced temperature gradient: a distortion inducing a variation of $(2X_2 - X_1 - X_3)$ equal to 5 nm is sufficient to explain the oscillating part of the phase drift.

This phase drift is not negligible with respect to the measured phase-shift Φ_0 and the phase without the nano grating is not a linear function of time. The mean of the two $X_G = 0$ phases measured just before and after the measurement done with the nano grating at X_G does not fully cancel this drift. In order to reduce the uncertainty on the nano grating induced phase-shift, for each gas velocity, we have made numerous measurements of the phase-shift. From the fits, we deduce for each measurement an error bar from which we calculate a weight used for a weighted average of the measurements. A χ^2 test is used to evaluate the 1σ error bar on this average. We have thus measured the phase Φ_0. The results, collected in Table 2, are plotted in Figures 4 and 5. As stated above, the measurements corresponding to the two highest velocities, which were made with second-order Bragg diffraction, are less satisfactory because of the existence of some stray beams due to residual first-order diffraction. In particular, for the phase measurements, the accuracy is less good than

for lower velocities, for which we have been able to reach an uncertainty below or near 3 mrad, which is 33 times smaller than in the similar experiment [9] done in 2005.

2.6 Phase noise

We have introduced the phase φ_{noise} to describe all the fluctuating phases (spatial fluctuations due to various atom trajectories or rapid temporal fluctuations due vibrations of the mirrors M_i [35]). The measured signal is an average of the distribution of φ_{noise}. Assuming that this distribution is even and centered around $\varphi_{noise} = 0$ so that $\langle \sin(\varphi_{noise}) \rangle = 0$, equation (1) becomes:

$$I = a_u^2 + a_l^2 + 2a_u a_l \cos(\varphi_0 + \Delta\varphi) \langle \cos \varphi_{noise} \rangle \quad (6)$$

where a_u and a_l are chosen real. This signal can be written in the usual form:

$$I = I_0 \left[1 + \mathcal{V}_0 \cos(\varphi_0 + \Delta\varphi)\right]. \quad (7)$$

Here I_0 is the mean intensity, $I_0 = a_u^2 + a_l^2$, $\mathcal{V}_0$ is the fringe visibility, $\mathcal{V}_0 = 2a_u a_l \langle \cos \varphi_{noise} \rangle / \left(a_u^2 + a_l^2\right)$ and φ_0 is the fringe phase of the unperturbed interferometer. The existence of a phase noise explains why the visibility $\mathcal{V}_0$ is smaller than its maximum value equal to 1, even when the two arms are perfectly balanced with $|a_u| = |a_l|$.

3 Model of the atom-surface interaction

We now turn to the theoretical prediction of complex diffraction amplitudes (modulus and phase) in the presence of atom-surface interactions. We discuss more specifically the case of the zeroth diffraction order and compare our experimental results to theory. We also obtain an analytic expression for the phase to explain the unusual velocity dependence. We finally discuss some alternative potentials such as a non-Newtonian modification to gravity.

3.1 Action of a nano grating on a plane wave

When a nano grating is introduced on an atomic beam represented as an incident plane wave $\Psi_i = \exp(i\mathbf{k} \cdot \mathbf{r})$, the array of equally spaced openings produces a series of beams corresponding to the various diffraction orders p_G. The transmitted wave Ψ_t is approximately given by:

$$\Psi_t = \sum_p A(p_G) \exp[i\mathbf{k} \cdot \mathbf{r}] \exp[i p_G \mathbf{k_G} \cdot (\mathbf{r} - \mathbf{r}_0)] \quad (8)$$

where $\mathbf{k_G}$ is the nano grating wavevector (a vector perpendicular to the nano grating lines, in its plane and of modulus $k_G = 2\pi/d$ where d is the nano grating period). $\mathbf{r_0}$ is a reference point in the nano grating plane and $A(p_G)$ is the diffraction amplitude of order p_G. The phase of $A(p_G)$ depends on the reference point $\mathbf{r_0}$ for all orders except for the zeroth order. Equation (8) is a good approximation near normal incidence when the diffraction angles are small i.e. when $k_G \ll k$.

The nano gratings used in atom optics experiments [33,34] are more complex with a periodic structure in two orthogonal directions: the nano grating in the $\mathbf{x}$ direction with a period d_x, typically equal to $d_x \sim 100$ nm, and a periodic support bar structure in the $\mathbf{y}$ direction with a larger period d_y, typically equal to $d_y \sim 1$ μm (Fig. 3). The nano grating axis $\mathbf{x}$ and $\mathbf{y}$ could be oriented in any direction in the $\mathbf{X}$, $\mathbf{Y}$ plane. We have chosen to put the $\mathbf{x}$ axis close to but not exactly coincident with the axis $\mathbf{Y}$ of the interferometer. We define two wave-vectors $\mathbf{k}_{Gx}$ in the $\mathbf{x}$ direction, with $k_{Gx} = 2\pi/d_x$ and $\mathbf{k}_{Gy}$ in the $\mathbf{y}$ direction, with $k_{Gy} = 2\pi/d_y$ and we must use two indices p_{Gx} and p_{Gy} to label the diffracted beams. Within the same approximations as above, the transmitted wave is now given by:

$$\Psi_t = \sum_{p_{Gx}, p_{Gy}} A(p_{Gx}, p_{Gy}) \exp[i\mathbf{k} \cdot \mathbf{r}] \times \exp[i\left(p_{Gx}\mathbf{k}_{Gx} + p_{Gy}\mathbf{k}_{Gy}\right) \cdot (\mathbf{r} - \mathbf{r_0})]. \quad (9)$$

3.2 Calculation of the diffraction amplitude, without atom-surface interaction

Let us first neglect the atom-surface interaction and, as in usual diffraction theory, assume that the grating bars perfectly absorb the incoming wave and that the wave is perfectly transmitted by the grating slits. Then, the diffraction amplitudes are directly related to the Fourier components of the transmitted wave. Assuming perfectly rectangular slits and taking the origin point $\mathbf{r}_0$ at the center of a slit, we get:

$$A(p_{Gx}, p_{Gy}) = \frac{\sin(p_{Gx}\pi\beta_x)}{p_{Gx}\pi} \frac{\sin(p_{Gy}\pi\beta_y)}{p_{Gy}\pi}. \quad (10)$$

β_x and β_y are the nano grating open fractions (i.e. the ratio of the size of the opening to the period) in the $\mathbf{x}$ and $\mathbf{y}$ directions, p_{Gx} and p_{Gy} label the diffraction orders. With our choice of origin, all these amplitudes are real. Equation (10) is valid if p_{Gx} and p_{Gy} are not equal to 0. When p_{Gx} or p_{Gy} vanishes, the ratio $\sin(p_{Gi}\pi\beta_i) / (p_{Gi}\pi)$ must be replaced by β_i so that $A(0,0) = \beta_x\beta_y$. In this approximation, the zeroth-order amplitude has a phase equal to zero, $\arg(A(0,0)) = 0$.

When we take into account the atom surface interaction below, we will only include the potential for the calculation of diffraction in the x direction. This is justified considering the opening width is only $w = 53$ nm. At this distance the effect of the van der Waals potential is significant. The size of the grating openings in the y direction is considerably larger, $\beta_y d_y \approx 1$ μm so the potential will be approximately constant along the y direction. We will assume that $A(0,0)$ is given by the product of the zeroth order amplitude β_y for diffraction in the $\mathbf{y}$ direction, and the (complex) diffraction amplitude in the $\mathbf{x}$ direction calculated below.

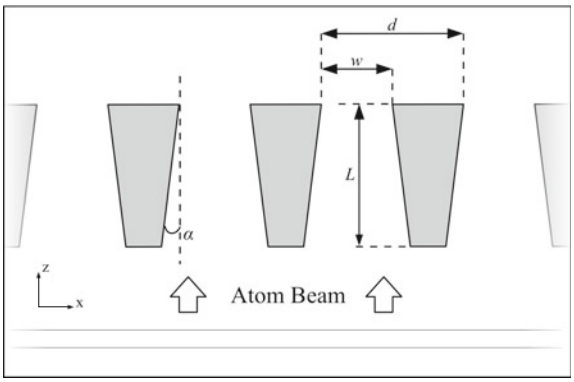

Fig. 7. A schematic representation of the nano grating geometry. The nano grating bars have a trapezoidal cross-section, with a wedge angle $\alpha = 5 \pm 1$ deg. The period of the nano grating is $d_y = 100 \pm 0.1$ nm and the period of the support structure is $d_x = 1.5$ μm. The width w of the nano grating windows is $w = 53 \pm 1.2$ nm. The thickness L of the bars is about $L = 110 \pm 5$ nm.

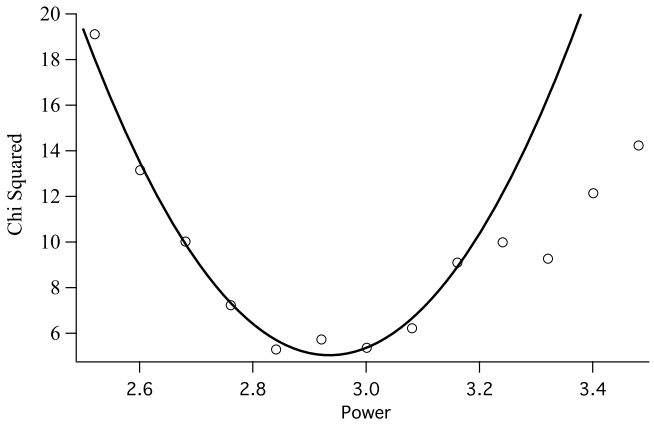

Fig. 8. The minimum of χ^2 found by fitting the data in Figure 5 using different values of p in equation (12). The values of χ^2 near the minimum are well described by a parabola with minimum at $p = 2.9$.

3.3 Diffraction amplitudes in the presence of atom-surface interactions

To explain the velocity dependence of the measured phase, we must consider the interaction of the atom with the nano grating in some detail. The atom-surface interaction potential is well known to have the form

$$V(r) = -\frac{C_p}{r^p}. \tag{11}$$

This formula is valid for an atom at a distance r from an infinite homogeneous half-space. We expect that $p \to 3$ for $r \ll \lambda/2\pi$ and $p \to 4$ for $r \gg \lambda/2\pi$, where λ is the resonance wavelength of the atom. For lithium $\lambda = 671$ nm, so that, $\lambda/2\pi = 107$ nm. Since the nano grating windows are 53 nm wide, the atoms propagate within ca. 25 nm of a surface. Furthermore, in the present experiment, the majority of the observed phase shift comes from atom-surface distances near 7 nm, as we will discuss near equation (20). We therefore expect $p = 3$.

An exact calculation of the potential viewed by an atom near a nano grating would be very complex. We will use the usual approximation [1,5] which replaces the exact potential between two grating bars by the potential due to two infinite half-spaces coincident with the two nearest walls. The potential is taken to vanish when the atom is outside of the grating. As the kinetic energy of the atoms is much larger than the atom-surface potential and the nano grating thickness is small enough, we will model the nano grating as a phase mask. As an atom passes with a velocity v through the nano grating, its wave-function acquires a position-dependent phase given in the WKB (or eikonal) approximation by:

$$\phi(x) = -\frac{1}{\hbar v}\int_{z_0}^{z_0+L} V(x,z)dz \tag{12}$$

where z is the direction of propagation, z_0 the coordinate of the nano grating entrance plane, x is the direction perpendicular to the nano grating bars and L is the thickness of the nano grating (see Fig. 7). The integral in equation (12) can be written as the sum of two terms representing the potential due to each of the two nearest walls:

$$\phi(x) = \phi_- + \phi_+. \tag{13}$$

For an atom-surface potential of the form in equation (11), the integral in equation (12) can be solved exactly to yield

$$\phi_\pm = \frac{C_p}{\hbar v}\frac{[L\tan(\alpha) + w/2 \pm x]^{1-p} - (w/2 \pm x)^{1-p}}{(1-p)\tan(\alpha)\cos^p(\alpha)} \tag{14}$$

where x is measured from the middle of a window (other parameters are defined in Fig. 7). A regularly spaced array of grating windows produces a diffraction pattern in the far field consisting of regularly spaced diffraction peaks. The complex amplitude of the p_{Gx}th diffraction order in the far field is now given by:

$$|A_{p_{Gx}}|e^{i\Phi_{p_{Gx}}} = \int_{-w/2}^{w/2} \exp\left[i\left(\phi(x) - \frac{2\pi p_{Gx}x}{d_x}\right)\right]dx \tag{15}$$

where d_x is the nano grating period in the $\mathbf{x}$ direction. The phase of the zeroth order diffraction amplitude is given by:

$$\Phi_0 = \arctan\left(\frac{\int_{-w/2}^{w/2}\sin[\phi(x)]\,dx}{\int_{-w/2}^{w/2}\cos[\phi(x)]\,dx}\right). \tag{16}$$

A numerical evaluation of this model using $p = 3$ matches the data in Figure 5 very well. For the geometric parameters of the grating we used the values from reference [6]. We also used different values of p to fit the data. The results of using $p = 2$ and $p = 4$ are also shown in Figure 5 and these results clearly disagree with our measured data. To determine the best value for p we repeated the fit in Figure 5 for several values of p and recorded the minimum in χ^2 found for each p. The results shown in Figure 8 are well described by a parabola that has a minimum for $p = 2.9$. The standard deviation associated with p is given

by the value of p for which $\chi^2 = \chi^2_{\min} + 1$ and, from this figure, we see $p = 2.9 \pm 0.2$.

The fit of our phase measurements in Figure 5 gives us $C_3 = (3.25 \pm 0.2)$ meV nm^3. While this value is very close to the value we would expect for lithium atom and a silicon nitride surface, we know that this grating has a thin gold-palladium metal coating on its surface. In addition, the C_3 coefficient has been measured for Na using the same grating [6]; the ratio between the two values $C_3(\text{Li})/C_3(\text{Na}) = 3.25/4.8 = 0.7$ is not very close to the ratio 0.9 we expect (see Appendix B). We discuss possible causes for this discrepancy below in Section 3.4.

As an additional check, we can fit the modulus of the transmitted amplitude to our model. The numerical evaluation of equation (15) using $p = 3$ and the fitted value of C_3 provides $|A_0|$ as a function of the atom velocity v. To compare this result with our measurement of $|A(0,0)|$, we must multiply it by the open fraction β_y in the **y** direction. We have fitted our measurements and obtained the best fit which gives $\beta_y = 0.61 \pm 0.01$, a value in reasonable agreement with a measurement based on SEM images of the grating, $\beta_y = 0.67 \pm 0.04$. The best fit is represented in Figure 6.

3.4 Comparison to theoretical prediction

We have evaluated several theoretical models for the atom-surface interaction. We have considered the interaction between Li and several different surfaces: a silicon nitride (SiN_x) surface (exploring different possible compositions), a bulk gold surface, and a SiN_x coated with a thin layer of gold. We know the grating has been covered with a thin layer of gold-palladium which can have a significant effect on the van der Waals potential strength. The details of these models are given in Appendix B. We give the results here in Table 3.

While we know the grating is coated with a thin layer of metal, the measured value of C_3 seems to be closer to the value for a pure SiN_x surface. In addition, the ratio between this measurement and a measurement of C_3 for Na using the same grating is smaller than we expect. There are several possible explanations for this. The reported value for C_3 is sensitively dependent on the geometry of the grating bars. It is possible that the characterization of the geometry in reference [6] was done on a slightly different region of the grating. Though the grating is fairly uniform, a 3 nm change to the width of the grating openings is sufficient to explain the discrepancy. It is also possible that the fringes formed by stray beams are not entirely washed out and that they contribute in a systematic way to the measured phase.

Though repeated measurements are reproducible, it cannot be ruled out that the different environments used for the current experiment and the one in [6] introduce different contaminations to the surface that affect C_3.

Several other physical phenomena may affect the individual C_3 values, as well as the ratio between the values obtained for Li and Na. The list of possibilities includes an oxide layer on the nanograting, contamination of the nanograting by the Na and Li atom beams, additional phase shifts due to propagation within the nanograting that cannot be modeled with the WKB (thin grating) approximation made in equation (12), different contributions to C_3 due to atomic core electrons, and also retardation. In particular, there should be different shifts due retardation for Li and Na because of their different resonance frequencies, and also due to the different distance ranges where the two different types experiments are most sensitive (approximately 7 nm for Li in the interferometer experiment [10] and 5 nm for Na in the diffraction experiments [6,9]). We have calculated the shifts in our measured C_3 due to each of these issues, and we conclude that every one of these possibilities would make a smaller shift than the uncertainty we still have due to the fact that the different experiments may have probed grossly different regions on the nanograting where the bars may be as much as 3 nm thicker or thinner. In the future, experiments such as the one in reference [8] can be designed to measure C_3 ratios more accurately to focus on these effects.

Table 3. Theoretical and experimental values of C_3 in meV nm^3. The theoretical calculations are based on various surface permittivities given in the associated references. Reference [40] also uses a different, more complete, model for atomic polarizability. Experimentally measured C_3 values for lithium are from our atom interferometer experiments (described in the present paper and reference [10]), and for sodium the measured C_3 comes from atom diffraction experiments described in reference [6]. Both sets of experiments use the same Au/Pd-coated SiN_x nanograting sample. See Appendix B for details.

Theory		
Surface	Na	Li
SiN_x [4]	3.17	2.95
Bulk Si_3N_4 [54]	3.34	3.10
SiN_x and 1-nm of Au [38]	4.30	3.82
Bulk Au [39]	4.93	4.50
Bulk Au [40]	5.47	4.88
Experiment		
Nanograting in interferometer [10]		3.25 ± 0.20
Nanograting and diffraction [6]	4.85 ± 0.50	

3.5 Analytical calculation of the diffraction amplitude and physical explanation of its velocity dependence

We have developed an analytic expression for the zeroth order phase, described in detail in Appendix A. The numerical model described above fits the Φ_0 data very well but it is interesting to try to understand the physical effects that cause its unusual velocity dependence.

Cronin and Perreault [7] have previously introduced a generalized Cornu spiral to visualize the integral in equation (15) and to predict the intensity of the various diffraction orders. We have used the same ideas to develop an analytical expression for the zeroth order amplitude $|A_0|e^{i\Phi_0}$.

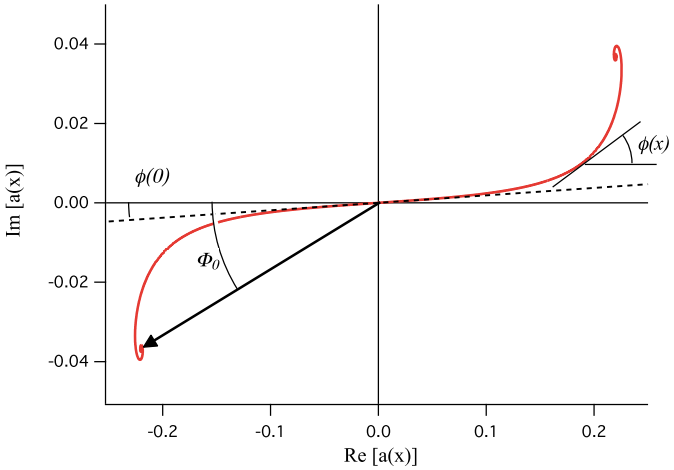

Fig. 9. (Online color) The Cornu spiral corresponding to the integral in equation (15). The vertical axis is scaled differently than the horizontal axis to exaggerate plotted angles. The total 0th order phase is dominated by the region near r_1 where $\phi(r_1) \approx 1$. The potential farther away from the wall is to weak the contribute significantly ($\phi(0) \ll \Phi_0$). The potential closer to the wall is so strong that it preferentially deflects atoms into higher diffraction orders. At these short distances the curvature of the Cornu spiral increases rapidly causing it to curl into a small spiral, thus no longer contributing significantly to Φ_0.

A plot of the Cornu spiral (Fig. 9) shows that the dominant contribution to this phase comes from the region where $|\phi(x)| \lesssim \pi/2$. To simplify the model, we consider square bars and the interaction with one of the nano grating walls only: this second assumption is justified by the fact that $\phi(0) \ll \Phi_0$. With these assumptions, the phase $\phi(x)$ is then given by:

$$\phi(x) = \frac{C_3 L}{\hbar v \left[(w/2) - x\right]^3}. \tag{17}$$

The calculation is detailed in Appendix A and we comment here only the results. The results are the first-order terms of an expansion in $r_1 = [C_3 L/(\hbar v)]^{1/3}$ which is the atom-surface distance such that $\phi(r_1) = 1$ rad. We get:

$$\Phi_0 \approx \frac{1.354 r_1}{w - 2.345 r_1}. \tag{18}$$

We can use this last result to explain the fact that Φ_0 is well approximated by a power law function of the atom velocity v, $\Phi_0 \propto v^q$. We calculate the log-derivative of Φ_0 with respect to v:

$$\frac{d\Phi_0}{\Phi_0} = -\frac{w}{3\left(w - 2.345 r_1\right)} \frac{dv}{v} \tag{19}$$

where we have used that $dr_1/r_1 = -dv/(3v)$. We thus expect a local power-law dependence of Φ_0 on v where the exponent q is given by

$$q = \frac{d\Phi_0}{\Phi_0} \Big/ \frac{dv}{v} = -\frac{w}{3\left(w - 2.345 r_1\right)} \approx -0.48 \tag{20}$$

where the numerical value is calculated with $r_1 = 7$ nm corresponding to the center $v \approx 1600$ m/s of the studied velocity range.

This velocity dependence for a phase shift in atom optics is unusual. A perturbation applied to one arm of an atom interferometer usually results in a phase shift proportional to v^{-1} while a gradient of an electric or magnetic field applied to both arms of an interferometer induces a phase shift proportional to v^{-2}. Geometric or topological phases, such as the Aharonov-Casher phase, are independent of velocity. Inertial forces due to acceleration and rotation of the interferometer with respect to a Galilean frame induce phase shift proportional respectively to v^{-2} and v^{-1}. The anomalous velocity dependence observed here is explained by the fact that the phase shift comes mostly from a region of atom-surface separation near r_1 which depends on the atom velocity and the similarity with $q = -1/2$ is simply a coincidence as shown clearly by equation (20). Instead the power q is related to the power p of the potential by $q = 1/p$ plus a correction which is a function of C_3, L and v.

3.6 Scaling of the experiment

It is worthwhile at this point to consider what would happen if we scaled this experiment to larger sizes of the grating windows. In particular, would it be possible to scale this experiment such that we can detect effects of retardation at distance ranges in the Casimir-Polder regime? For Li, we expect to see deviations from the $V \propto r^{-3}$ law at a distance of about 107 nm.

We have demonstrated the ability to measure VdW induced phases of about 0.1 radians, we will therefore require that the phase induced by a larger nano structure be at least this large. We discussed in the previous section that the experiment is most sensitive to an atom-wall separation of r_1. Though r_1 is not directly dependent of the window width w, we must have $r_1 < w/2$. Therefore, a requirement to be able to measure atom-surface potentials at larger distances is that the grating windows are larger. From equation (18) we can see that for large windows the measured phase goes approximately as $1/w$, not as $1/w^3$ which one might naively expect. Larger nanostructures would therefore still produce a significant phase shift. If we want $r_1 \approx 100$ nm and $\Phi_0 \approx 0.1$ we see that $w < 1500$ nm would be acceptable.

The experiment is most sensitive to a range of atom-surface separations near r_1. At longer distances, the potential is so weak that it does not contribute significantly to the measured phase shift; at shorter distances the potential is so strong that atoms are deflected away from the detector. To get $r_1 = 107$ nm, we must increase the ratio L/v by a factor of 3500. Nano-structures that have $L = 2$ μm are currently available, for these gratings we need atoms traveling at a velocity of 10 m/s to see the effect of retardation. Such velocities are currently not attainable by supersonic sources, but are achievable in cold atom experiments.

Using supersonic sources, velocities of 500 m/s may be attainable (some novel methods can even attain 250 m/s [37]). For these velocities nano structures that are about 1 mm thick would be required. Under these two extreme conditions, one should question if the approximations used in the current analysis are still valid. The above discussion assumes the atom beam is coherent over the width of a grating window. In the case of a beam that is (mostly) uncollimated in the **Y** direction, like in the current experiment, the coherence length in the **Y** direction is much less than the proposed 1 μm window width. As a consequence, such gratings would produce a signal with significantly reduced contrast.

3.7 Test of possible modification of Newton's law of gravitation at short distances

The precision of our measurement can be used to test the existence of other interactions at short length scales. Many works have been devoted to the test of possible modifications of Newtonian gravity at various length scales [41–45]. The potential energy between two point masses m_1 and m_2 is commonly assumed to be given by a Yukawa type term:

$$U(r) = \frac{Gm_1m_2}{r}\left[1 + \alpha \exp\left(-r/\lambda\right)\right]. \qquad (21)$$

G is Newton's gravitational constant and r is the distance between the masses. α and λ measure the amplitude and the range of the non-Newtonian alteration of the gravitational energy. Accordingly, the Newtonian expression is recovered either by putting $\alpha = 0$ (purely Newtonian interaction), or for a given $\alpha \neq 0$, by letting $\lambda \to 0$ (infinitely small range).

It is straightforward to verify that the purely Newtonian part of the interaction is totally negligible in our experiment, so we will focus on the non-Newtonian term. Just like in the case of the van der Waals phase shift discussed above, we replace the exact potential by the one created by two infinite half-spaces coincident with the two nearest nano grating walls, when the atom is in the channel between two nano grating bars, and zero everywhere else. This approximation is good as long as the range λ is small with respect to the bar thickness equal to $(d_x - w) \approx 47$ nm in our experiment. Then, if μ is the density of the grating material and m_1 the mass of the atom, a straightforward integration proves that the non-Newtonian potential is given by:

$$U(x) = 2\pi G m_1 \mu \alpha \lambda^2 \times \left[\exp\left[\left(\frac{w}{2} - x\right)/\lambda\right] + \exp\left[\left(\frac{w}{2} + x\right)/\lambda\right]\right]. \qquad (22)$$

In order to simplify this formula, we have neglected the wedge angle of the grating bars and the potential is thus independent of z, as long as the atom is between the grating bars ($0 < z < L$). However, all the numerical calculations have taken the wedge of the grating bars into account and we use equation (12), but replace the van der Waals term V by the sum $V + U$.

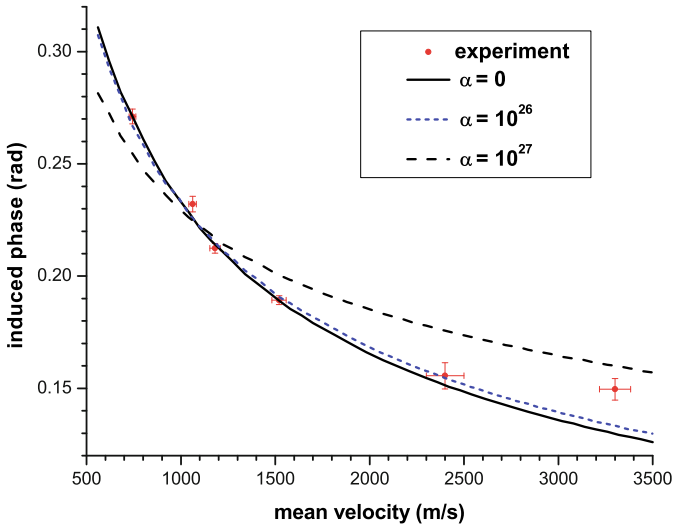

Fig. 10. (Color online) Phase Φ_0 of the zeroth order diffraction amplitude as a function of the atomic beam mean velocity v. Three different fits of Φ_0 are made with different values of the the amplitude α of the Non-Newtonian gravitational potential, with a fixed range $\lambda = 2$ nm: the full curve corresponds to $\alpha = 0$ and the best fit gives $C_3 = 3.25$ meV nm^3; the short-dashed (blue) curve corresponds to $\alpha = 10^{26}$ and the best fit gives $C_3 = 3.12$ meV nm^3 and this fit is as good as the fit with $\alpha = 0$; the long-dashed (black) curve corresponds to $\alpha = 10^{27}$ and the best fit gives $C_3 = 2.55$ meV nm^3 and this last fit is clearly less good than the the two previous ones and the C_3 value is clearly too low.

Using the silicon nitride bulk density $\mu = 3270$ kg/m^3 and the Newton constant $G = 6.67 \times 10^{-11}$ m^3 kg^{-1} s^{-2}. we determine the maximum $|\alpha|$ value compatible with the measured phase shifts, by using a fit with α and C_3 as free parameters, while the range λ is fixed. We show in Figure 10 fits of the measured phase Φ_0 of the zeroth order diffraction amplitude, assuming various values of the amplitude α of the Non-Newtonian gravitational potential, with a fixed range $\lambda = 2$ nm. From this series of fits, we can set a limit on the amplitude α for this range, $|\alpha| \lesssim 10^{26}$.

We have made similar calculations for a range $\lambda = 1$ and 10 nm and our results are plotted in Figure 11 where they are compared with previous experiments based on macroscopic force measurements [46]. The constraint on $|\alpha|$ is less strict than the previously published results except for a range $\lambda = 2$ nm, where it is almost exactly the same, $|\alpha| \lesssim 10^{26}$. To improve this limit, we could enhance the modified gravitational potential with respect to the van der Waals term. This could be done by using a heavier atom and a more dense grating material without increasing C_3 too much. Using cesium atoms will enable to use laser diffraction and using a gold (coated) grating material would enhance the product $m_1\mu$ by a factor 112. Because cesium has a larger electric polarizability than lithium and because gold is metallic, the C_3 coefficient would be 3 times larger than for the lithium-SiN_x interaction. The experiment can be even farther improved by

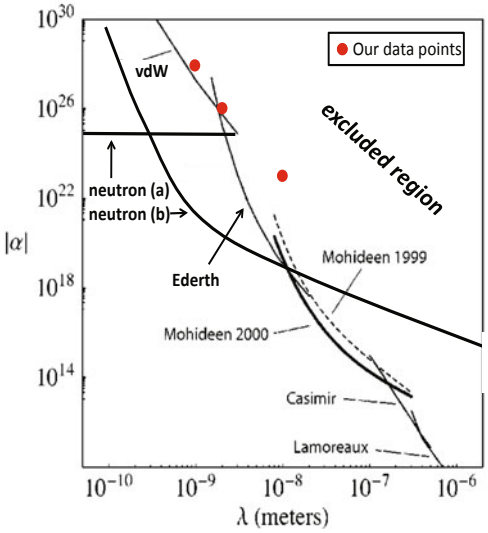

Fig. 11. (Color online) Constraint on the α parameter of the Yukawa potential describing a possible modification of Newtonian at short range as a function of the range parameter λ. The full dots (red online) represent the maximum $|\alpha|$ value compatible with our phase shift measurements calculated assuming $\lambda = 1$, 2 and 10 nm. This figure copied from Fischbach et al. [46] presents the limit obtained by several macroscopic force experiments of Israelachvili and Tabor [47] (curve labeled vdW) and by Ederth [48] (curve labeled Ederth) (see Ref. [46] for more details). When $\lambda = 1$ or 10 nm, our limit on $|\alpha|$ is less strict than previous measurements but when $\lambda = 2$, our limit is competitive with these macroscopic measurements. Finally, the neutron data is taken from Figure 28 of the review by Abele [49] who plots in an α-λ diagram the results of reference [50].

using an atom like xenon which has a mass similar to cesium but a VdW interaction that is 10 times smaller.

Neutron optics and collision experiments have given more stringent constraints on α for λ values in the nanometer range. In the review of Abele [49], Figure 28 presents limiting α values derived from a reanalysis of existing data by Leeb and Schmiedmayer [50]. For a range $\lambda < 10^{-8}$ m, these constraints are up to several orders of magnitude stronger than those derived from experiments involving atoms or solids interacting with solids. This is easy to explain by the fact that the electric polarizability α_n of neutron [49] is many orders of magnitude smaller those of atoms ($\alpha_n \approx 10^{-48}$ m^3 as compared to the one of lithium atom $\alpha_{Li} = 2.43 \times 10^{-29}$ m^3). The extremely low electric polarizability of neutron makes that its VdW interaction with matter is negligible and the only important interaction of neutron with matter is the short range nuclear interaction. With experiments involving atoms or solids interacting with solids, the limits on an hypothetical non-Newtonian gravitational interaction at short range correspond to the case where the van der Waals interaction and the non-Newtonian gravitational interaction are of comparable magnitudes.

4 Conclusion

We summarize the main results of this paper:

- We have used the Toulouse atom interferometer to measure the zeroth order diffraction amplitude of lithium waves by a nano grating made of silicon nitride. Thanks to some technical improvements, we have been able to measure the modulus and the phase of this amplitude with an uncertainty close to 1% for most of the data points. Most of the measurements have been done with our interferometer using first order Bragg diffraction, but we have also used second order Bragg diffraction in some cases in order to enhance the distance between the interferometer arms. Even if the accuracy was less good in this case, the prospect of using higher order Bragg diffraction is very interesting as it opens up many possibilities.
- The phase measurements exhibit an unexpected dependence with the atom velocity, roughly like $v^{-0.49}$. We have developed a numerical model and an approximate analytical calculation which explain this velocity dependence. The zeroth order diffraction amplitude is calculated by integrals similar to those appearing in the Cornu spiral and the dominant contributions come from an atom-surface distance which is a function of the atom velocity. This explains why the effect of the atom-surface potential cannot be understood by a simple perturbation calculation which would predict a v^{-1} velocity dependence.
- The high accuracy of our measurements has enabled us to test the dependence of the atom-surface interaction with distance. Our data is consistent with a $-C_p/r^p$ potential only if $p = 2.9 \pm 0.2$, in good agreement with theory which predicts that, in the range of distance tested by our experiment around 10 nm, the van der Waals potential behaves as $-C_3/r^3$.
- Using accurate determinations of the grating geometrical parameters deduced from a series of diffraction experiments [6], we used phase data to determine $C_3 = 3.25 \pm 0.2$ meV nm^3. This value is in good but not exact agreement with our calculation using a well-established theoretical formula and an accurate description of the atom and surface optical properties. The small disagreement is probably due to a 1 nm thick gold-palladium coating deposited on the grating for STM imaging purposes.
- We have used the same data to test a possible modification of the gravitation potential at short range. If this modification is described by a Yukawa potential, our experiment achieves a sensitivity comparable to best published results for a range of the Yukawa term equal to $\lambda = 2$ nm, at least if we except the experiments

involving neutron interferometry. It seems possible to improve our results by a factor of the order of 10 this sensitivity by using a denser material for the grating and, if possible, a heavier atom.

A more general remark concerns the extraordinary sensitivity achieved by atom interferometry with separated arms. We are now able to measure phase-shifts with a few milliradians error bar and this uncertainty is not limited by fundamental effects but by an uncontrolled phase drift which should be reduced in an improved experiment. The detection of extremely weak interactions is at hand.

S.L., H.J., G.T., M.B. and J.V. thank CNRS INP, Région Midi-Pyrénées and ANR (grant ANR-05-BLAN-0094) for support. VPAL and ADC acknowledge financial support from NSF grant No. 0969348.

Appendix A: Analytic calculation of the zeroth-order amplitude in a simplified geometry

We want to calculate the zeroth-order diffraction amplitude given by equation (15):

$$|A_0|e^{i\Phi_0} = \frac{1}{d_x}\int_{-w/2}^{w/2} \exp\left[i\phi(x)\right] dx. \tag{A.1}$$

As $\phi(x)$ is an even function of x, we can write $|A_0|e^{i\Phi_0} = I_c + iI_s$ with:

$$\begin{aligned} I_c &= \frac{2}{d_x}\int_0^{w/2} \cos[\phi(x)]dx \\ I_s &= \frac{2}{d_x}\int_0^{w/2} \sin[\phi(x)]dx. \end{aligned} \tag{A.2}$$

To simplify the calculation, we take the wedge angle of the grating $\alpha = 0$ and we consider the interaction with only one of the nano grating walls, so that $\phi(x)$ is given by equation (17). We can now write the phase acquired along a straight path through the grating in terms of two dimensionless parameters, $U = 2x/w$ and $A = 2r_1/w$, where $r_1 = [C_3 L/(\hbar v)]^{1/3}$ (r_1 is the atom-surface distance for which $\phi(x) = 1$ rad). The phase ϕ becomes

$$\phi(U) = \left(A/(1-U)\right)^3. \tag{A.3}$$

If $A = 0$ (i.e. $C_3 = 0$), then $I_c = w/(2d_x)$ and $I_s = 0$. When $C_3 \neq 0$, the first corrections are linear in r_1 and we calculate here only these first-order terms. We begin by writing

$$\begin{aligned} I_s &= \frac{w}{d_x}\int_0^1 \sin\phi(U)dU \\ I_c &= \frac{w}{d_x}\int_0^1 \cos\phi(U)dU. \end{aligned} \tag{A.4}$$

We now use ϕ as the new integrating variable and, for I_s, we get:

$$\begin{aligned} I_s &= \frac{Aw}{3d_x}\int_{A^3}^{+\infty} \phi^{-4/3}\sin(\phi)d\phi \\ &\approx \frac{Aw}{2d_x}\Gamma\left(\frac{2}{3}\right) = \frac{r_1}{d_x}\Gamma\left(\frac{2}{3}\right). \end{aligned} \tag{A.5}$$

We have used results from reference [51,52] and we have kept only the term linear in A. For I_c, we only calculate the linear term in the Taylor expansion of equation (A.2). To this end, we must calculate the derivative of I_c with respect to A at $A = 0$ and we find:

$$\left.\frac{\partial I_c}{\partial A}\right|_{A=0} = -\frac{w}{d_x}\int_0^{+\infty} \phi^{-1/3}\sin(\phi)d\phi = -\frac{w\sqrt{3}}{2d_x}\Gamma\left(\frac{2}{3}\right).$$

We thus get I_c up to its first order term in A:

$$I_c \approx \frac{w}{d_x}\left[1 - \frac{\sqrt{3}}{2}\times\Gamma\left(\frac{2}{3}\right)A\right] \tag{A.6}$$

substituting $wA = 2r_1$ we get

$$I_c \approx \frac{w}{d_x} - \frac{r_1\sqrt{3}}{d_x}\Gamma\left(\frac{2}{3}\right). \tag{A.7}$$

The zeroth order amplitude phase Φ_0 is approximately given by $\Phi_0 \approx I_s/I_c$ and we finally get:

$$\Phi_0 \approx \frac{\Gamma\left(\frac{2}{3}\right)r_1}{w - \sqrt{3}\times\Gamma\left(\frac{2}{3}\right)r_1} \approx \frac{1.354 r_1}{w - 2.345 r_1} \tag{A.8}$$

where $\Gamma(2/3) \approx 1.354$. The modulus $|A_0|$ of the zeroth order amplitude is approximately given by $|A_0| = \sqrt{I_c^2 + I_s^2}$ with I_c and I_s given by equations (A.7) and (A.7). A slightly less accurate result is obtained by keeping only the first order term in r_1, with $|A_0| \approx I_c \approx \left[w - r_1\sqrt{3}\Gamma(2/3)\right]/d_x$.

Appendix B: Calculation of the atom-surface C_3 coefficient

We calculate the van der Waals C_3 coefficient describing the interaction of a silicon nitride surface with various atoms: two alkali Li and Na, the rare gases He, Ne, Ar, Kr, Xe and also the D_2 molecule. We also calculate C_3 for Li near a silicon nitride surface coated with a uniform layer of gold. All these C_3 coefficients have been measured by atom optics and/or interferometry [1,9]. We start from the result of Lifshitz [28] and of Zaremba and Kohn [29]:

$$C_3 = \frac{1}{4\pi}\int_0^{\infty} \alpha(i\omega)g(i\omega)d\omega \tag{B.1}$$

where $\alpha(i\omega)$ is the atomic dynamic polarizability and $g(i\omega)$ is the surface response function, in both case for

imaginary frequency. $g(i\omega)$ is related to the solid electric permittivity by:

$$g(i\omega) = \frac{\varepsilon(i\omega) - 1}{\varepsilon(i\omega) + 1}. \tag{B.2}$$

Vidali and Cole [53] proposed to use approximate Lorentzian forms for $\alpha(i\omega)$ and $g(i\omega)$:

$$g(i\omega) = g_0 / \left[1 + \frac{(\hbar\omega)^2}{E_s^2}\right] \tag{B.3}$$

g_0 is dimensionless, $0 < g_0 < 1$, and E_s is the mean dipolar excitation energy of the solid.

$$\alpha(i\omega) = \alpha_0 / \left[1 + \frac{(\hbar\omega)^2}{E_d^2}\right] \tag{B.4}$$

α_0 is the atom static electric polarizability and E_d its mean dipolar excitation energy. From equations (B.1), (B.3) and (B.4), Vidali and Cole obtained a closed form expression of C_3:

$$C_3 = \frac{g_0 \alpha_0 E_d E_s}{8(E_d + E_s)}. \tag{B.5}$$

To obtain a more accurate value of C_3 we are going to evaluate the function $\epsilon(i\omega)$ from measurements of the complex index of refraction $n + ik$ of Si_3N_4 [54]. We get the real and imaginary parts of $\varepsilon = \varepsilon_1 + i\varepsilon_2$ by $\varepsilon_1 = n^2 - k^2$ and $\varepsilon_2 = 2nk$, which are plotted in Figure 12. For the following calculations, we must interpolate $\varepsilon_1(\omega)$ and $\varepsilon_2(\omega)$ by sufficiently regular analytic functions. In 1996, Jellison and Modine [55] have proposed to represent ε_2 by the following Tauc-Lorentz (TL) formula:

$$\varepsilon_{2TL}(E) = \frac{AC E_0 (E - E_g)^2}{(E_0^2 - E^2)^2 + C^2 E^2} \frac{1}{E}, \text{ when } E > E_g$$
$$\varepsilon_{2TL}(E) = 0, \text{ when } E \leq E_g \tag{B.6}$$

where E_g is the band-gap energy, while A, C, and E_0 are respectively the strength, the spectral width and the center of the resonance (all these quantities are in units of energy). Using the Kramers-Kronig relations, an analytic expression for ε_{1TL} can be found as demonstrated by Jellison and Modine [55].

Using the commercial software Origin, we have fitted the Tauc-Lorentz formula $\varepsilon_{2TL}(E)$ to the available data over its complete energy range and we have obtained $A = 242.5 \pm 7.3$ eV, $C = 5.93 \pm 0.07$ eV, $E_g = 5.19 \pm 0.04$ eV, $E_0 = 8.18 \pm 0.06$ eV. As shown in Figure 12, this fit is very good. Then, assuming $\varepsilon_{1TL}(\infty) = 1$, we have introduced these parameters in the formula for $\varepsilon_{1TL}(E)$ and, as shown by Figure 12, the agreement with the measured values of $\varepsilon_1(E)$ is very good too.

The same Tauc-Lorentz formula was used by Savas to describe the complex permittivity of the LPCVD silicon nitride SiN_x he used to manufacture nano gratings [3]: he obtains very different values of the parameters $A = 74.5$ eV, $C = 7.62$ eV, $E_g = 2.29$ eV and

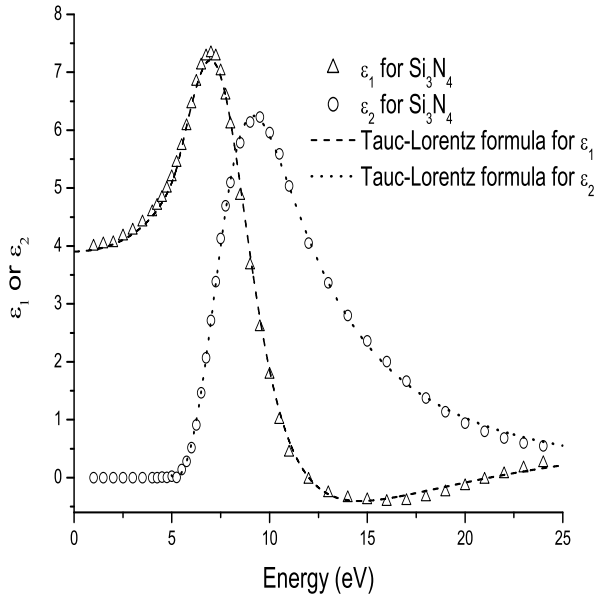

Fig. 12. Plots of the real and imaginary parts ε_1 and ε_2 of the complex dielectric permittivity of bulk Si_3N_4 as a function of the photon energy in eV. The data points are experimental while the curves represent the fit using the Tauc-Lorentz formula (see text).

$E_0 = 7.17$ eV and these differences are probably due to the non-stoichiometric character of the SiN_x membrane. We will use these two sets of parameters to describe silicon nitride permittivity, in order to have an idea of the effect of the variation of the surface properties. As our nano grating has also been produced by Savas, we expect that the data for LPCVD silicon nitride SiN_x should give the best results.

We can now deduce the dielectric constant at imaginary frequencies $\varepsilon(i\omega)$ by the Kramers-Kronig relation [56,57]:

$$\varepsilon(i\omega) = 1 + \frac{2}{\pi} \int_{\omega_g}^{\infty} \frac{\xi\, \varepsilon_{2TL}(\xi)}{\xi^2 + \omega^2} d\xi. \tag{B.7}$$

We have used the commercial software Mathematica to calculate the integral of equation (B.7) and the results are plotted in Figure 13.

For the atomic polarizability, we have used the single oscillator model given by equation (B.4) for all the atoms and for D_2 molecule. In addition we used a two-oscillator model for lithium as well. The static electric polarizability α_0 and the mean dipolar excitation energy E_d were taken from Tang et al. [58] for the rare gases, and from Kramer and Herschbach [59] for D_2. For lithium and sodium, we use the most accurate calculated values of the electric polarizability, $\alpha_0(\text{Li}) = 164.111$ a.u. [60] and $\alpha_0(\text{Na}) = 162.6$ a.u. [61] respectively with E_d from [58]. Table 4 compares experimental and calculated values of C_3 coefficients and the agreement is good in almost all cases: the agreement is usually better with the calculation using the thin film SiN_x electric permittivity except for Na

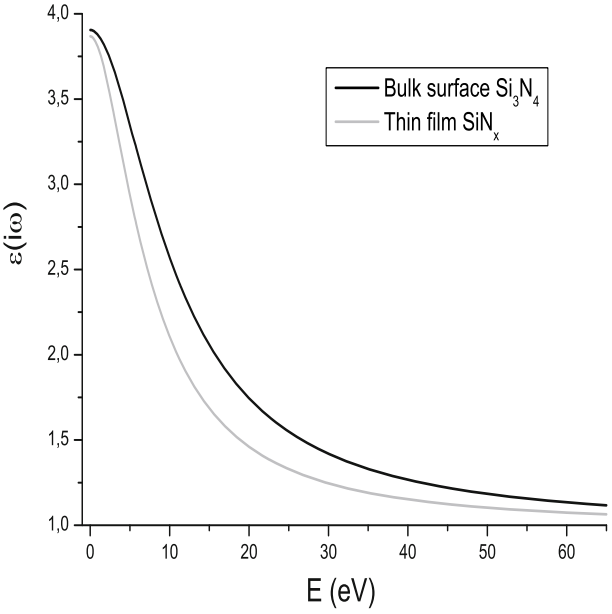

Fig. 13. Plot of dielectric constant $\varepsilon(i\omega)$ of silicon nitride for imaginary frequency, as function of the photon energy $\hbar\omega$: the full curve describes the bulk Si_3N_4, with the parameters fitted in the present paper and the dashed curve describes the thin film SiN_x, with the parameters fitted by Savas and quoted in reference [3].

and Li, since these two measurements were done with a grating that has a thin metal coating.

For lithium, the total oscillator strength of the first resonance transition is considerably lower than 1, $f_1 = 0.747$ [62] and we cannot neglect higher excitation transitions. We must write the electric polarizability in the form:

$$\alpha(i\omega) = \sum_j \frac{f_j}{\omega_j^2 + \omega^2}. \tag{B.8}$$

For lithium, the resonance transition explains 98.68% of the calculated electric polarizability [60] and the remaining transitions with $\sum_{j\neq 1} f_j = 0.253$ contribute only to 1.32% of the static polarizability because their frequencies ω_j are in the UV. Following equation (B.5), the relative contribution of these transitions is expected to be larger to C_3 than to the static polarizability. As discussed by Jacquey in her thesis [63], the knowledge of the oscillator strengths of the Rydberg states and of the continuum is not very good. Here, we replace all these contributions by a second effective oscillator with $f_{eff} = 0.253$ and $\hbar\omega_{eff} = 9.19$ eV, chosen such that the static polarizability is conserved. The results of this new calculation appear in Table 4: C_3 increases by about 3%.

To evaluate C_3 for Li and Na near a bulk gold surface we used a Drude model for the permittivity

$$\varepsilon_{Au}(i\omega) = 1 + \frac{\omega_p^2}{\omega^2 + \gamma\omega} \tag{B.9}$$

Table 4. Comparison between experimental and calculated values of C_3 in meV nm^3. Experimental C_3 values are from reference [1] for H_2 and the rare gases, from our experiment (present paper and Ref. [10]) for lithium and from reference [6] for sodium. The calculations differ by the choice of the Tauc-Lorentz parameters describing silicon nitride (see text). For lithium, we present the results of two calculations, with a single-oscillator model (a) and with a two-oscillator model (b) for the atom. For bulk Au we present our calculated value (see text), and we also tabulate the value calculated in [40] (c).

Species	Experiment	Calculation Bulk Si_3N_4	Calculation Thin film SiN_x
D_2	0.35 ± 0.06	0.51	0.42
D_2	0.31 ± 0.07		
He	0.10 ± 0.02	0.15	0.122
Ne	0.22 ± 0.04	0.25	0.212
Ar	0.71 ± 0.12	0.86	0.736
Kr	1.09 ± 0.18	1.18	1.01
Li (a)	3.25 ± 0.20	3.00	2.86
Li (b)		3.10	2.95
Na (a)	4.85 ± 0.30	3.34	3.17
Species	Experiment	Calculation Bulk Au	Calculation SiN_x 1 nm Au
Li	3.25 ± 0.20	4.50	3.82
Li (c)		4.88	
Na	4.85 ± 0.50	4.93	4.30
Na (c)		5.47	

where the ω_p is the plasma frequency and γ is a damping constant. The values of C_3 obtained from this formula with $\hbar\omega_p = 6.36$ eV and $\hbar\gamma = 26$ meV are listed in Table 4.

Our metal coated grating consists of a thin coating of a Au/Pd mixture on top of the silicon nitride nano-bars. In modeling such a system we must take into account the interface between the vacuum and the thin outer surface as well as the interface between the surface layer and the underlying bulk material. To do this, we have evaluated expression 4.14 in reference [64]. We used a Drude model for $\epsilon_{\mathrm{Au}}(i\omega)$ and a simple insulator model for $\epsilon_{\mathrm{SiN}_x}(i\omega)$. The results are shown in Table 4.

References

1. R.E. Grisenti, W. Schöllkopf, J.P. Toennies, G.C. Hegerfeldt, T. Köhler, Phys. Rev. Lett. **83**, 1755 (1999)
2. R.E. Grisenti, W. Schöllkopf, J.P. Toennies, G.C. Hegerfeldt, T. Köhler, M. Stoll, Phys. Rev. Lett. **85**, 2284 (2000)
3. R. Brühl, P. Fouquet, R.E. Grisenti, J.P. Toennies, G.C. Hegerfeldt, T. Köhler, M. Stoll, Walter, Europhys. Lett. **59**, 357 (2002)
4. R. Brühl, R.P. Fouquet, R.E. Grisenti, J.P. Toennies, G.C. Hegerfeldt, T. Köhler, M. Stoll, C. Walter, Europhys. Lett. **59**, 357 (2002)
5. J.D. Perreault, A.D. Cronin, T.A. Savas, Phys. Rev. A **71**, 053612 (2005)

6. V.P.A. Lonij, W.F. Holmgren, A.D. Cronin, Phys. Rev A **80**, 062904 (2009)
7. A.D. Cronin, J.D. Perreault, Phys. Rev. A **70**, 043607 (2004)
8. V.P.A. Lonij, C.E. Klauss, W.F. Holmgren, A.D. Cronin, Phys. Rev. Lett. **105**, 233202 (2010)
9. J.D. Perreault, A.D. Cronin, Phys. Rev. Lett. **95**, 133201 (2005)
10. S. Lepoutre, H. Jelassi, G. Trénec, M. Büchner, J. Vigué, V.P.A. Lonij, A.D. Cronin, Europhys. Lett. **88**, 20002 (2009)
11. A.D. Cronin, J. Schmiedmayer, D.E. Pritchard, Rev. Mod. Phys. **81**, 1051 (2009)
12. C.R. Ekstrom, J. Schmiedmayer, M.S. Chapman, T.D. Hammond, D.E. Pritchard, Phys. Rev. A **51**, 3883 (1995)
13. A. Miffre, M. Jacquey, M. Büchner, G. Trénec, J. Vigué, Phys. Rev. A **73**, 011603(R) (2006)
14. B. Deissler, K.J. Hughes, J.H.T. Burke, C.A. Sackett, Phys. Rev. A **77**, 031604(R) (2008)
15. J. Schmiedmayer, M.S. Chapman, C.R. Ekstrom, T.D. Hammond, S. Wehinger, D.E. Pritchard, Phys. Rev. Lett. **74**, 1043 (1995)
16. T.D. Roberts, A.D. Cronin, D.A. Kokorowski, D.E. Pritchard, Phys. Rev. Lett. **89**, 200406 (2002)
17. M. Jacquey, M. Büchner, G. Trénec, J. Vigué, Phys. Rev. Lett. **98**, 240405 (2007)
18. H. Hoinkes, Rev. Mod. Phys. **52**, 933 (1980)
19. D. Bloch, M. Ducloy, Adv. At. Mol. Opt. Phys. **50**, 91 (2005)
20. J.D. Perreault, A.D. Cronin, Phys. Rev. A. **73**, 033610 (2006)
21. J.D. Perreault, A.D. Cronin, J. Phys. Conf. Ser. **19**, 146 (2005)
22. P.W. Milonni, *The Quantum Vacuum* (Academic, New York, 1994)
23. V. Druzhinina, M. DeKieviet, Phys. Rev. Lett. **91**, 193202 (2003)
24. T.A. Pasquini, Y. Shin, C. Sanner, M. Saba, A. Shirotzek, D.E. Pritchard, W. Ketterle, Phys. Rev. Lett. **93**, 223201 (2004)
25. J.M. McGuirk, D.M. Harber, J.M. Obrecht, E.A. Cornell, Phys. Rev. A **69**, 062905 (2004)
26. D.M. Harber, J.M. Obrecht, J.M. McGuirk, E.A. Cornell, Phys. Rev. A **72**, 033610 (2005)
27. J.M. Obrecht, R.J. Wild, M. Antezza, L.P. Pitaevski, S. Stringari, E.A. Cornell, Phys. Rev. Lett. **98**, 063201 (2007)
28. E.M. Lifshitz, Sov. Phys. JETP **2**, 73 (1956)
29. E. Zaremba, W. Kohn, Phys. Rev. B. **13**, 2270 (1976)
30. A. Miffre, M. Jacquey, M. Büchner, G. Trénec, J. Vigué, Eur. Phys. J. D **33**, 99 (2005)
31. Q. Turchette, D. Pritchard, D. Keith, J. Opt. Soc. Am. B **9**, 1601 (1992)
32. C. Champenois, M. Büchner, J. Vigué, Eur. Phys. J. D **5**, 363 (1999)
33. C.R. Ekstrom, D.W. Keith, D.E. Pritchard, Appl. Phys. B **54**, 369 (1992)
34. T.A. Savas, S.N. Shah, M.L. Schattenburg, J.M. Carter, H.I. Smith, J. Vac. Sci. Technol. B **13**, 2732 (1995)
35. A. Miffre, M. Jacquey, M. Büchner, G. Trénec, J. Vigué, Appl. Phys. B **84**, 617 (2006)
36. S. Vieira, IBM J. Res. Dev. **30**, 553 (1986)
37. E. Narevicius, A. Libson, M.F. Riedel, C.G. Parthey, I. Chavez, U. Even, M.G. Raizen, Phys. Rev. Lett. **98**, 103201 (2007)
38. B.S. Zhao, S.A. Schulz, S.A. Meek, G. Meijer, W. Schöllkopf, Phys. Rev. A **78**, 010902 (2008)
39. M.A. Ordal, L.L. Long, R.J. Bell, R.R. Bell, R.W. Alexander Jr., C.A. Ward, Appl. Opt. **22**, 1099 (1983)
40. G. Lach, M. Dekieviet, U.D. Jentschura, Int. J. Mod. Phys. A **25**, 2337 (2010)
41. S. Dimopoulos, A.A. Geraci, Phys. Rev. D **68**, 124021 (2003)
42. S.K. Lamoreaux, Phys. Rev. Lett. **78**, 5 (1997); erratum, Phys. Rev. Lett. **81**, 5475 (1998)
43. R.S. Decca, D. Lopez, H.B. Chan, E. Fischbach, D.E. Krause, C.R. Jamell, Phys. Rev. Lett. **94**, 240401 (2005)
44. D.J. Kapner, T.S. Cook, E.G. Adelberger, J.H. Gundlach, B.R. Heckel, C.D. Hoyle, H.E. Swanson, Phys. Rev. Lett. **98**, 021101 (2007)
45. A.A. Geraci, S.J. Smullin, D.M. Weld1, J. Chiaverini, A. Kapitulnik, Phys. Rev. D **78**, 022002 (2008)
46. E. Fischbach, D.E. Krause, V.M. Mostepanenko, M. Novello, Phys. Rev. D **64**, 075010 (2001)
47. Y.N. Israelachvili, D. Tabor, Proc. R. Soc. Lond. A **331**, 19 (1972)
48. T. Ederth, Phys. Rev. A **62**, 062104 (2000)
49. H. Abele, Prog. Part. Nucl. Phys., **60**, 1 (2008)
50. H. Leeb, J. Schmiedmayer, Phys. Rev. Lett. **68**, 1472 (1992).
51. I.S. Gradshteyn, I.M. Ryzhik, *Tables of integrals, series and products*, 4th edn. (Academic Press, 1980)
52. *Handbook of Mathematical Functions With Formulas, Graphs, and Mathematical Tables*, Applied Mathematics Series, edited by M. Abramowitz, I.A. Stegun (National Bureau of Standards, 1964), p. 55
53. G. Vidali, M.W. Cole, Surf. Sci. **110**, 10 (1981)
54. H.R. Philipp, *Handbook of Optical Constants of Solids I*, edited by E.D. Palik (Academic, New York, 1985), p. 771
55. G.E. Jellison Jr., F.A. Modine, Appl. Phys. Lett. **69**, 371 (1996); erratum, Appl. Phys. Lett. **69**, 2137 (1996)
56. L.D. Landau, E.M. Lifshitz, L.P. Pitaevskii, *Electrodynamics of Continuous Media* (Butterworth-Heinemann, 1984)
57. A. Lambrecht, S. Reynaud, Eur. Phys. J. D **8**, 309 (2000)
58. K.T. Tang, J.M. Norbeck, P.R. Certain, J. Chem. Phys. **64**, 3063 (1976)
59. H.L. Kramer, D.R. Herschbach, J. Chem. Phys. **53**, 2792 (1970)
60. Z.-C. Yan, J.F. Babb, A. Dalgarno, G.W.F. Drake, Phys. Rev. A **54**, 2824 (1996)
61. M.S. Safronova, W.R. Johnson, A. Derevianko, G.W.F. Drake, Phys. Rev. A **60**, 4476 (1999)
62. Z.-C. Yan, G.W.F. Drake, Phys. Rev. A **52**, R4316 (1995)
63. M. Jacquey, Ph.D. thesis, Université P. Sabatier, 2006, available on http://tel.archives-ouvertes.fr/
64. F. Zhou, L. Spruch, Phys. Rev. A **52**, 297 (1995)